



OPEN

SUBJECT AREAS:

MECHANICAL
ENGINEERING

BIOMINERALIZATION

Received
12 November 2013Accepted
24 January 2014Published
20 February 2014

Correspondence and
requests for materials
should be addressed to
P.R.L. (prleduc@cmu.
edu) or W.C.M.
(william.messner@
tufts.edu)

Controlling Magnetotactic Bacteria through an Integrated Nanofabricated Metallic Island and Optical Microscope Approach

Lina M. González¹, Warren C. Ruder³, Philip R. Leduc^{1,2} & William C. Messner^{1,4}

¹Department of Mechanical Engineering, Carnegie Mellon University, Pittsburgh, PA, USA, ²Biomedical Engineering, Computational Biology, and Biological Sciences, Carnegie Mellon University, Pittsburgh, PA, USA, ³Department of Biological Systems Engineering, Virginia Tech, Blacksburg, VA, USA, ⁴Department of Mechanical Engineering, Tufts University, Medford, MA, USA.

Herein, we demonstrate the control of magnetotactic bacteria through the application of magnetic field gradients with real-time visualization. We accomplish this control by integrating a pair of macroscale Helmholtz coils and lithographically fabricated nanoscale islands composed of permalloy ($\text{Ni}_{80}\text{Fe}_{20}$). This system enabled us to guide and steer amphitrichous *Magnetospirillum magneticum* strain AMB-1 to specific location via magnetic islands. The geometries of the islands allowed us to have control over the specific magnetic field gradients on the bacteria. We estimate that magnetotactic bacteria located less than $1\ \mu\text{m}$ from the edge of a diamond shaped island experience a maximum force of approximately 34 pN, which engages the bacteria without trapping them. Our system could be useful for a variety of applications including magnetic fabrication, self-assembly, and probing the sensing apparatus of magnetotactic bacteria.

Controlling magnetic field gradients while simultaneously imaging biological and non-biological magnetic specimens will contribute to scientific fields ranging from magnetic fabrication^{1,2} to probing the behavior of magnetotactic bacteria³. A number of techniques currently exist to create and manipulate magnetic fields including magnetic tweezers⁴, magnetic needles⁵, and permanent magnets⁶. Each of these systems provides distinct ways to apply magnetic fields and exert forces for magnetic manipulation. Magnetic manipulation tools join the repertoire of tools, such as optical tweezers and atomic force microscopy (AFM), for making measurements like the contour and persistent length of DNA molecules and the strength of cellular adhesion forces^{4,7–9}.

Magnetic techniques are often preferred over optical techniques¹⁰ for force application because magnetic fields provide a way to non-invasively manipulate cells without excessive heating. Many researchers have attached commercially available functionalized magnetic beads to cells to examine such cellular properties and functions as elasticity and mechanotransduction^{11–13}. In biology, there has been a growing interest in organisms like magnetotactic bacteria (MTB), because they naturally synthesize chains of magnetic particles and this unique feature makes them guidable to specific locations¹⁴. A significant drawback of optical tweezers is that the local heating can irreversibly denature proteins and damage living cells. Although magnetic fields applied at low frequencies ($<100\ \text{Hz}$) typically do not generate significant heat in biological samples, heat may be generated in magnetic coils themselves. When the magnetic coils are located at a distance from the sample, such as with Helmholtz coils, the generated heat can be removed by convective cooling with liquid¹⁵ or gas¹⁶ before it affects the sample.

In this paper, we present an approach that combines macroscale Helmholtz coils and lithographically fabricated nanoscale islands composed of permalloy ($\text{Ni}_{80}\text{Fe}_{20}$) to control magnetotactic bacteria as well as magnetic particles (Fig. 1a–c). These nanoscale islands concentrate magnetic fields generated by the Helmholtz coils, and the resulting magnetic field gradients apply forces on the magnetotactic bacteria. The system controls applied forces and moments and enables the precise positioning and orientation of magnetic particles as well as being able to steer motile magnetotactic bacteria. In comparison to techniques like magnetic tensile cytometry (MTC)¹⁷, which also uses concentrated magnetic field gradients, the use of nanoscale magnetic islands bypasses the need for the bulk pole pieces (i.e., large needles) typically used to generate magnetic field gradients¹⁸ and can create arrays of islands for high throughput control of magnetotactic motility. The advantage of our approach is applying

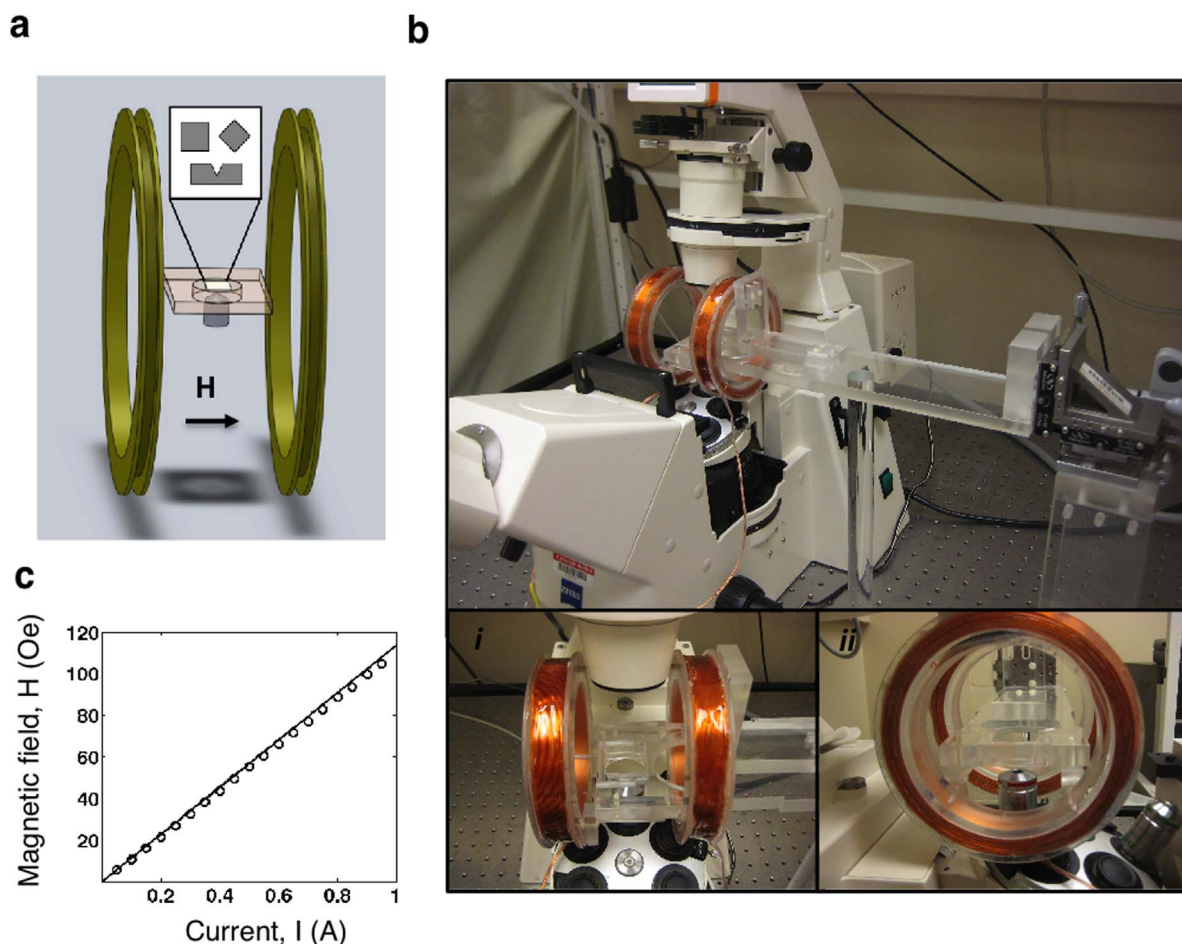


Figure 1 | Integrated nanofabricated metallic island and optical microscope for control magnetic fields on magnetic particles and magnetotactic bacteria. (a) Schematic of experimental set-up: Helmholtz coils integrated with nanofabricated permalloy ($\text{Ni}_{80}\text{Fe}_{20}$) islands. (b) Custom-built pair of Helmholtz coils to fit an inverted microscope for magnetizing the permalloy island. Inset (i) is a front view of the Helmholtz coils and the specimen holder. Inset (ii) is a side view of the Helmholtz coils (c) Characterization of the Helmholtz coils showing magnetic field strength versus applied current to the Helmholtz coils.

physics to biology by building a system that controls magnetotactic bacteria. This capability is of great interest to many areas including (in the short term) investigating the behaviors and mechanisms of magnetotactic bacteria (MTB) and (in the much the longer-term) the idea of creating sentinel robotic systems that could be directed with drug treatments, etc., in the body through controlling magnetic fields. While the latter is in the very long term, it is interesting since these organisms are non-pathogenic and naturally respond to magnetic fields. This system described here may impact multiple areas of research ranging from directed magnetic self-assembly to the investigation of magnetically responsive organisms¹⁹ and magnetically based drug release systems²⁰.

Results

In order to create the magnetic field concentrators for integration with the Helmholtz coils (Fig. 1), we fabricated thin permalloy metallic islands. Figure 2a is a schematic of the fabrication process for the permalloy islands (Fig. 2b; see Material and Methods section for a detailed description of fabrication of these islands). To visualize the interaction of AMB-1 with these islands using a $63\times$, 1.4 N.A., oil immersion objective in an inverted microscope, the islands and the microscope slide thickness could not exceed $170\ \mu\text{m}$, and when the thickness of the metal layer was less than $30\ \text{nm}$, the metal layer was optically translucent. This fabrication approach allowed us to visualize the bacteria and magnetic particles on top of the islands. In

order to exert higher forces on the beads, we also nanofabricated islands four times thicker than the $30\ \text{nm}$ islands ($120\ \text{nm}$).

Forces on the magnetic beads and the magnetotactic bacteria. We examined our system through simulations (Fig. 3a, b, top panels) and experimentally compared these using ferromagnetic particles made from uniform polystyrene spheres coated with chromium dioxide ($4.5\ \mu\text{m}$ in diameter; Spherotech Inc.; see supplementary material for the code used to run these simulations). These particles permitted us to map the magnetic field gradients and quantify the forces imparted on the magnetic particles by these islands. The ferromagnetic particles moved to the areas of high magnetic field concentration (Fig. 3b, bottom panels, Movies S1 and S2). The beads moved to the regions predicted by finite element method magnetics modeling (Fig. 3b, top panels). We obtained magnetic hysteresis curves to provide important information such as magnetization (from which the magnetic susceptibility was determined) and the coercivity for our approach. The magnetic hysteresis of the magnetic beads and the permalloy film were acquired using an alternative gradient force magnetometer (AGFM) (MicroMag Model 2900; Princeton Measurements Inc.) and exhibited coercive forces (H_c) of $567\ \text{Oe}$ (in agreement with other studies²¹) and $14\ \text{Oe}$, respectively (Fig. 3c, d). Our results were in line with the known low coercive force of this permalloy²². This magnetic hysteresis also indicated that there was little magnetic remanence remaining in the islands once a field was removed.

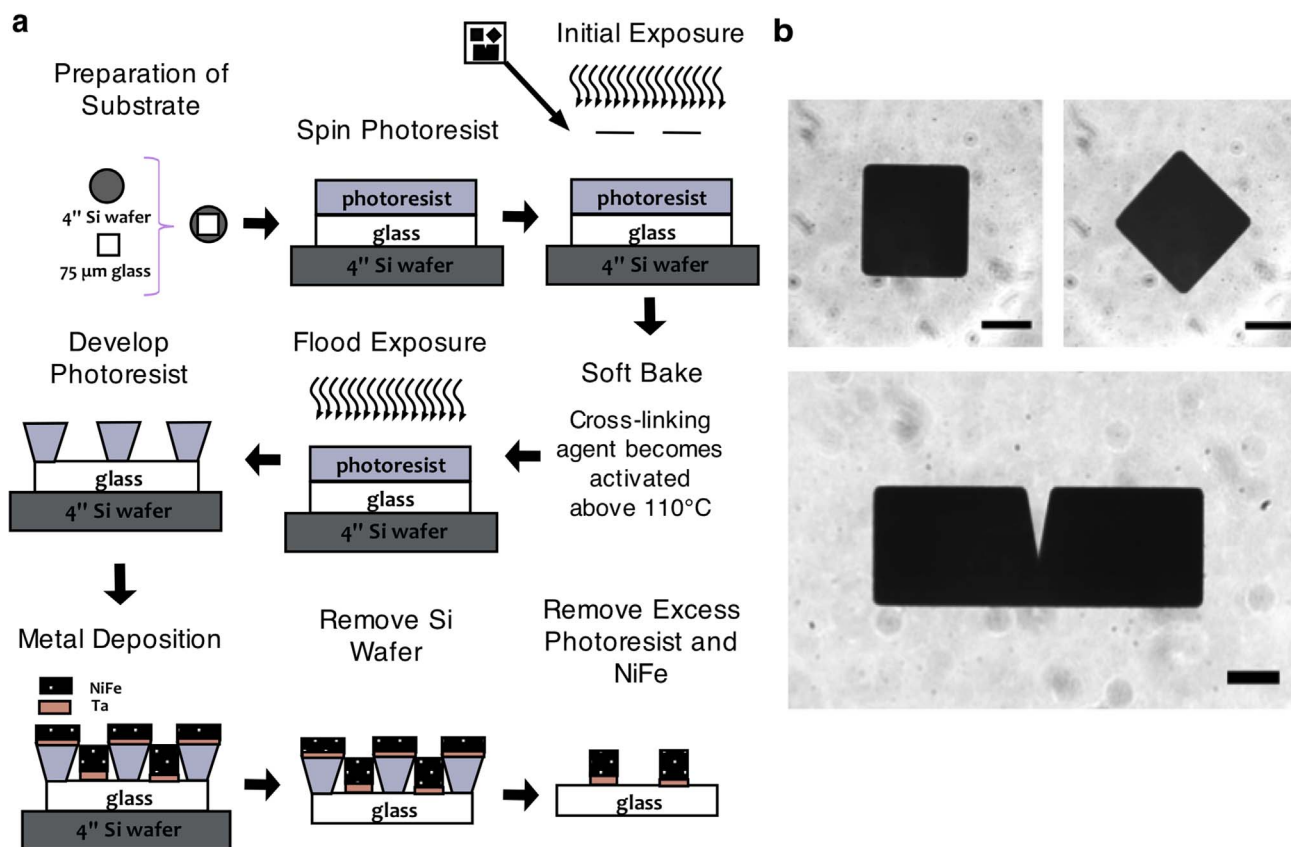


Figure 2 | Fabrication of permalloy islands to make magnetic concentrators. (a) The image reversal fabrication steps implemented to make permalloy islands of controlled geometries. (b) Bright field microscope images of different shapes of the permalloy islands fabricated using the image reversal method. Scale bar, 10 μm .

To quantify the forces exerted by the islands on the beads, we applied Newton's second law and the balance of magnetic and drag forces (see supplementary material for equations). Using in-house code written in MATLAB, we determined the magnetic forces exerted on the beads by tracking them. Figure 4 shows the magnetic force with respect to the distance to the edge or vertex in the vicinity of the square and diamond islands. We also varied the thickness of the island, and found that increasing the thickness from 30 nm to 120 nm subsequently increased the magnetic force by approximately 50% (Fig. 4). Generally, islands with larger areas and volumes exert more forces on the beads, which is consistent with theory predicting that magnetic force is directly proportional to the volume of the magnetic material. Furthermore, we found that the diamond-shaped island (which are the same area as the square) with its shape anisotropy created higher gradients.

In addition, we calculated the forces on the magnetic bacteria by extrapolating data from the magnetic beads forces that we have previously calculated. We used a similar approach to calculate the force exerted on these magnetotactic bacteria by the magnetized islands. To do this, we used the magnetic hysteresis (of the beads and magnetotactic bacteria, Fig. S1) and the forces vs. distance curves. From the magnetic hysteresis we calculated the magnetic susceptibility. From the force versus distance curves, we determined the forces on the beads very close to the islands' edge (see the supplementary material for details of the calculations and equations used). Assuming that the biogenic magnetic particles (BMP) are $1.9 \times 10^{-15} \text{ m}^2$ (50 nm in diameter) in cross-sectional area and that the chains have a maximum chain length of about 2 μm (a cells is typically around 3 μm) we estimate that very close to the edge (approximately 3 μm), the magnetic forces on the AMB-1 starts to increase exponentially and reach a maximum of 34 pN (Fig. 5). Figure 5 also

shows the effect of increasing the length of the magnetosome chain. For instance, a cell with a chain that is only 0.5 μm would experience 10 fN (femto Newton) at 1 μm away, however a cell with a magnetosome chain that is 2 microns in length would experience 10 fN at about 2 μm away. The maximum force on the magnetosome chains by the diamond island of sizes 0.5 μm , 1 μm , 1.5 μm and 2 μm is approximately 8 pN, 16 pN, 25 pN and 34 pN, respectively.

Guiding the cells using the notch and diamond shape islands. We used our magnetic field concentrators to affect the motion of living organisms as well. Since magnetotactic bacteria sense and respond to the magnetic field of the Earth, we applied a localized magnetic field gradient to motile AMB-1. While magnetic particles passively move to locations of the steepest magnetic field gradients, the bacteria actively swim in response to the magnetic field gradients. One interesting observation was the deflecting behavior (Fig. 6, left panel), which we attributed to the “bridging” of the magnetic field lines across the “notch-shaped” islands as shown in Figures 6a–b, Figure S2 and Movie S3. In Figures 6c, d, and e, the deflection of the AMB-1 away from and near the notched part of the island revealed distinct deflection responses when using a very low external field (3 Oe). Near the notch region, this deflection varies from 0 to approximately 50° from the x-axis (Fig. 6d, black symbols) whereas in the upstream region the AMB-1 cells tend to orient to a lesser degree (0– 30°). (Fig. 6e, black symbols). These data suggest that near the notch region the cells are deflecting their motility paths to follow the magnetic field lines. These deflection patterns are different than that of the control (when we apply no external magnetic field) as the cells are showing wider spread of deflections in both upstream and near the notch regions (Fig. 6d and e, blue symbols). These results are important because the method could one

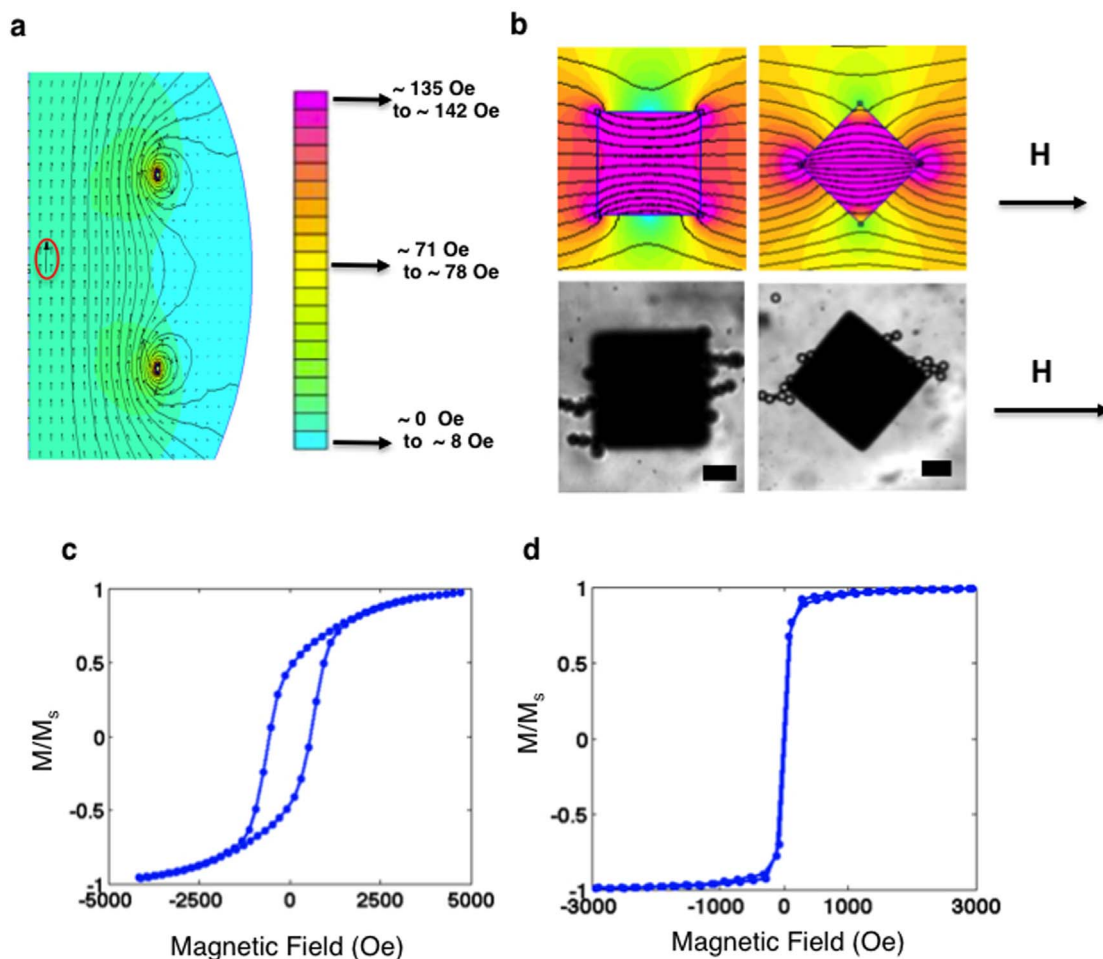


Figure 3 | Characterization of the permalloy island and magnetic bead response. (a) A two-dimensional field intensity profile of the application of magnetic fields on the permalloy islands through our Helmholtz coils simulated using finite element method magnetics (FEMM). The red circle represents the approximate area of homogenous magnetic field where the permalloy islands are placed in the simulation. (b) Simulation results of the islands with applied external magnetic fields from the Helmholtz coils of about 80 Oe (top). Experimental comparison of these concentrated magnetic field regions through tracking ferromagnetic bead movement with the applied magnetic field (bottom). Scale bar, 10 μm . Magnetic hysteresis loop of the ferromagnetic beads and permalloy film using an alternative gradient force magnetometer (AGFM). (c) AGFM hysteresis loop of the ferromagnetic beads with a coercive field of 567 Oe and (d) AGM hysteresis loop of the permalloy films with a coercive field of 14 Oe. Both magnetic hysteresis curves are normalized by the moment.

day supplant conventional magnetic particle inspection techniques (MPI)²³.

Moreover, we were able to control the movement of the AMB-1 using the diamond island. The cells are able to move along the edge of this island, following it, until reaching a point of a low field or an area of a corner where the bacteria then moves away from the diamond (Fig. 6, right panel). The island used here is 120 nm thick, and the external field strength is 120 Oe. For example, in Figure 6 h–m (Movie S4) when the external magnetic field is on, a MTB gets directed toward one of the magnetic island vertices labeled as “Engaging zone” (this is where the field is the highest based on our simulations; Fig. 6f). This MTB is motile, and so it is actively moving, but it is moving in a directed fashion. The bacterium appears to follow the edge of the island until it reaches another vertex labeled as “Escape zone” (the field is lowest in this area based on our simulations; Fig. 6f). Thus, we were able to guide the cells (at an angle from the external magnetic field) to specific points near the islands, which is a significant capability for directing the bacteria.

To further quantify these effects, we analyzed the videos and determined that $30\% \pm 10$ (s. d.) ($n = 83$) of the cells swimming near these diamonds island (we examined a $60 \mu\text{m}$ by $40 \mu\text{m}$ region enclosing the diamond island) effectively altered their direction toward the

edge of the islands. The cells that were pulled towards to the edge were the ones that were the closest to the edge. We also quantified the distance between the cells and the islands when the cells were influenced by the magnetic field (the moment at which they lose independence in swimming), which was $3.6 \mu\text{m} \pm 1.4$ (s. d.)

Discussion

We used our microscope nanofabrication approach to control the motility of magnetotactic bacteria (Fig. 6). This control was enabled by implementing a combination of a single pair of Helmholtz coils and nanofabricating magnetic permalloy islands. Here the external magnetic field produced by the coils influences the cells to move from left to right or right to left within the field of view of the microscope. Thus the external field magnetically induces their orientation. The direction of movement of MTB is also controlled when using static Helmholtz coils and different geometries of the magnetic permalloy islands. These provide local control through local field gradients. These movements are influenced by the re-orientation due to the localized magnetic fields coupled with the velocity of the flagella enabled swimming bacteria. The distance that the cells needed to engage with the edge of the diamond island was below $3.6 \mu\text{m}$. This distance coincides with the rapid increase of the field (Fig. 5).

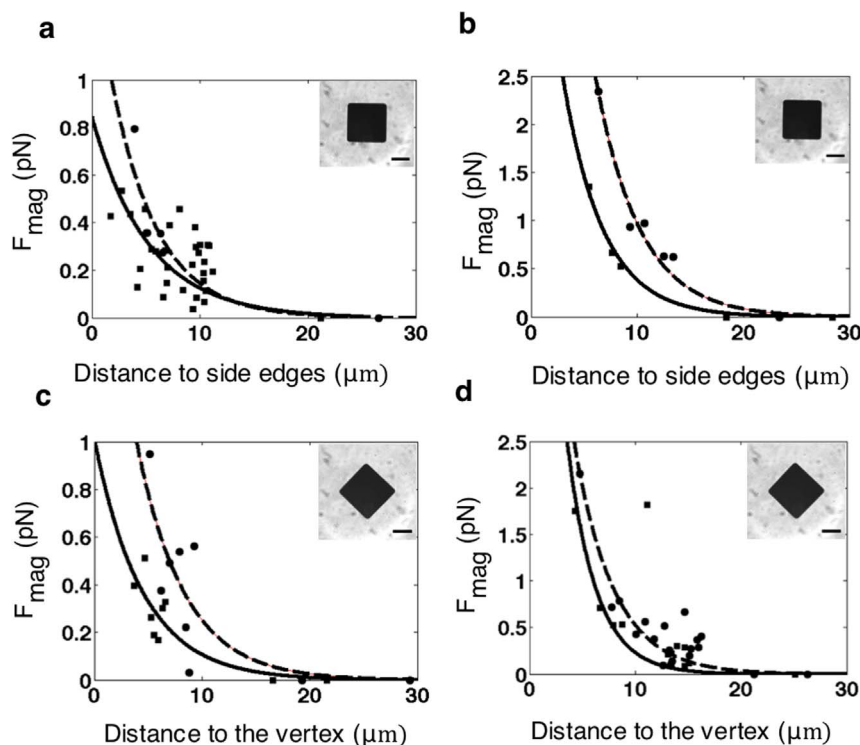


Figure 4 | Force versus distance results for the square- and diamond- shaped magnetic islands with an applied magnetic field. The square and circles represent the data for fields equal to 40 G and 120 G, respectively. (a–b) Force due to square island with height equal to 30 nm and 120 nm. (c–d) Force due to the diamond island with height equal to 30 nm and 120 nm.

To increase the area or volume near the edge that effectively engages the cells, the system could be influenced by changing parameters such as: increasing the current to the coils from the power supply, increasing the volume (either the area or the thickness) of the island, and by having the cells being more magnetically responsive. This could be accomplished through connecting power supplies in series or growing the cells under strict anaerobic condition (e.g. by degaussing their culturing medium).

This system could also be used to calculate the forces exerted by the flagella by considering three limiting cases. If the *M. magneticum* strain AMB-1 are swimming away from the island, and at a critical distance from the island, AMB-1 can no longer resist the magnetic force then $F_{\text{flagella}} = F_{\text{mag}}$. Closer to the island than the critical distance, F_{mag} will be greater than F_{flagella} , and the magnetic force will

pull microorganism towards the island. The third limiting case occurs when the bacteria overcomes the magnetic forces exerted by the islands ($F_{\text{mag}} < F_{\text{flagella}}$). However, this calculation could only be made in an ideal case scenario, and it is more complicated than looking at the limiting cases because the cells may be slowing down due to environmental cues as they response to many difference signals. The force on the AMB-1 about 2 μm from the edge of the diamond is about 10 fN (assuming the length of the chain is 2 μm long). The estimated maximum force of 34 pN is in indirect agreement with the estimate force on the flagella motor of other species (*Escherichia coli* and *Salmonella Typhimurium*) which is about 1500 pN²⁴. This force of 34 pN is sufficient to engage the cells, but not to complete immobilized them thus we can effectively guide these cells.

One important potential future concept from these additional studies is that these islands could be used in single cell manipulation to screen MTB with weak and strong magnetic chains by sorting them with an array of diamond shape islands position diagonally from each other such as to a compartment in a microfluidic channel device. Such arrays of islands could also be potentially used in directed evolution by trapping the cells repeatedly.

To conclude, we developed a custom-designed system integrating Helmholtz coils and nanofabricated magnetic islands for applying controlled magnetic fields and field gradients. We used this system to control the movement of magnetic particles and to study the behavior of magnetotactic bacteria. Straightforward modifications of this system are possible to exert higher forces and would be useful for studying cells and other organisms that sense magnetic fields. Our work has implications for several fields including magnetic self-assembly, physiological response to magnetic fields, and research on organisms containing magnetic particles.

We would like to thank Carson Kline for his initial help in the NanoFab. The authors would also like to thank Andrew Gamble for help with measuring the hysteresis loops and Dr. Sara Majetich for helpful comments on the manuscript. This work was supported in

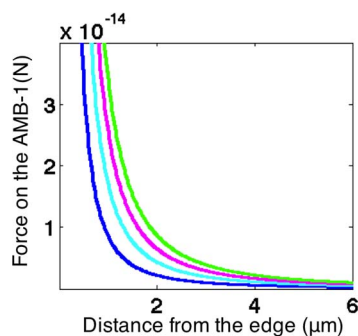


Figure 5 | Forces on the magnetosomes from the islands and the effect on increasing the magnetosome chains size. (a) The force vs. distance curve distance curves indicate the different sizes in the magnetosome chain of 0.5 (blue), 1 (cyan), 1.5 (magenta) and 2 (green) microns in length. The surface area is fixed and is 1.9×10^{-15} (50 nm in diameter). The forces on the magnetosome increase exponentially within a few microns from the edge of the island.

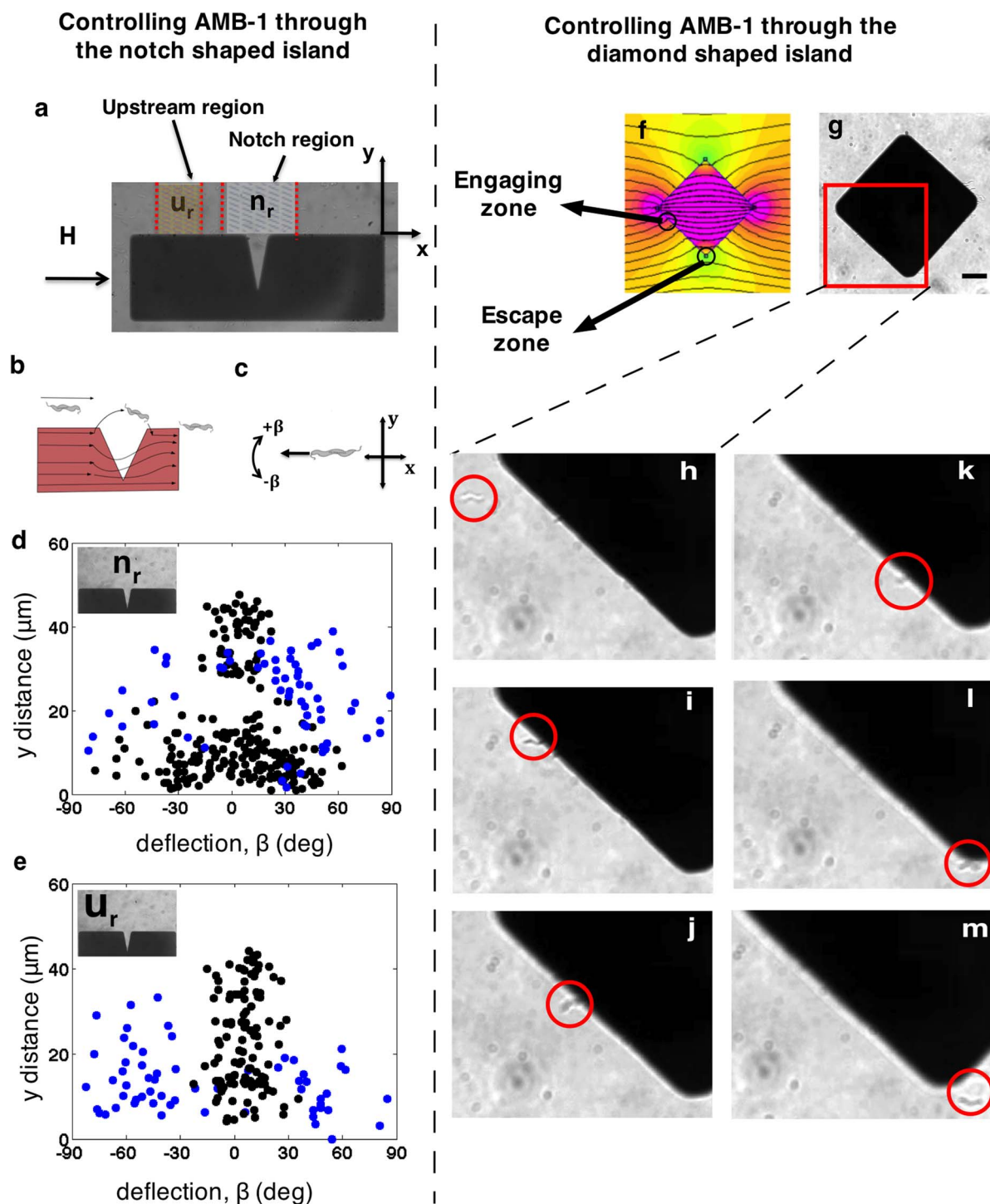


Figure 6 | MTB interactions with notch and diamond islands. (Left panel) MTB were tracked as they moved from the upstream region to the notch region. (a) Figure showing the different regions (upstream and notched regions). (b) Schematic showing the magnetic field lines near the notch island. (c) A schematic of the coordinates to track the deflection. Orientation of the MTB when they are upstream of the notch, n_r (d) and as they approach the region above the notch, u_r (e) when compared to vertical distance (y) away from the islands. The field corresponding to d–e is 3 Oe and the thickness of the island is 30 nm. (Right panel). The black symbols represent the bacteria when a field is applied and the blue symbols represent the bacteria when there is no external magnetic field. (Right panel) This panel shows the movement of MTB along the edge of the diamond island. (f) FEMM simulation of the diamond magnetic island showing the differences in the field between the “engaging” and “escape” zones. (g) A micrograph of the diamond island, which is 120 μm in thickness and the external magnetic field is 120 Oe. (Scale bar, 5 μm). (h–m) Image sequences of the magnetotactic bacteria moving along the edge of the diamond island. The bacterium (highlighted with a red circle) moves toward the engaging zone and glides along the edge (as in a “rail”) of this island until moving away from the island at the escape zone.



part by the National Science Foundation (CMMI-1100430, CMMI-1160840, CPS-1135850), the Office of Naval Research (N000140910215), the Sloan Foundation, and the Air Force Office of Scientific Research (FA9550-13-1-01 08), as well as a National Science Foundation Graduate Research Fellowship under Grant No. 0946825 to L.M.G.

Methods

Construction and characterization of Helmholtz coils. The Helmholtz coils in our system produce a uniform magnetic field with field lines concentrated within the permalloy islands. The governing equation used to calculate the forces on the magnetic particles is equation 1 although it can be found in other forms with the assumption that the initial magnetization of the magnetic beads is negligible^{25,26}.

$$F = (m \cdot \nabla) B \quad (1)$$

To develop an approach for manipulating magnetic samples including magnetic particles and magnetotactic bacteria, we first custom designed a pair of Helmholtz coils for a conventional inverted microscope (Zeiss Axiovert 200) as shown in Figure 1. The axis of these coils was positioned perpendicular to the optical axis. This pair of Helmholtz coils consisted of two identical coils separated by the radius of the coils. We designed and fabricated a custom stage that held the samples and the Helmholtz coils through an L-shaped piece attached to a micromanipulator (Newport, M-462) (Fig. 1b). The frames of the Helmholtz coils and stage were made of poly (methyl-methacrylate) (PMMA). We used a pair of miniature cooling fans to prevent excessive Joule-heating. The radius of the coils were 4.5", and the gauge of the magnet wire used was 22 AWG (American wire gauge). This pair of Helmholtz coils had 400 turns in each coil, and the windings were stacked in 7 layers. The magnetic field was measured using a gaussmeter (Lakeshore, Model 410). To characterize the magnetic field, B , at the center location of the coils, we used equation 2:

$$B = \left(\frac{4}{5}\right)^{3/2} \frac{\mu_0 NI}{R} \quad (2)$$

where N is the number of turns, μ_0 is the permeability constant, I is the applied current, and R is the radius of the coils. Figure 1c depicts the characterization of the field with respect to the current.

Fabrication of the custom-made metallic magnetic islands for an inverted microscope.

A 150 μm glass wafer (Mark Optics Inc.) served as the microscope slide. The image reversal technique resulted in a negative image of the mask pattern, allowing for effective lift-off of the metal film after fabrication²⁷. Using heat-releasing double-sided tape (release point = 150°C), a thin, fragile glass wafer was attached to a stronger silicon wafer for generating the islands. Bis(trimethylsilyl)amine (HMDS) was spun onto the glass/silicon wafer sandwich twice at 4000 rpm for 45 s. HMDS is an adhesive promoter commonly used to adhere photoresist to a glass wafer. A positive photoresist, AZ5214E-IR (MicroChem), was spun onto the surface at 4000 rpm for 45 s. The wafer was soft-baked at 95°C for 60 s to dry the solvent. During the initial exposure, the resist was controllably exposed to ultra-violet (UV) light through a photomask with an intensity of 150 mJ/cm² for 50 s. The photomask was a chrome quartz mask with a tolerance of 0.5 μm , which enabled us to repeatedly fabricate sharp features. To activate the crosslinking agent exposed to the UV light, the wafer was incubated at 105°C and 115°C on hotplates for 30 s and 120 s, respectively. During the flood exposure, the wafer was exposed to UV light without the mask at 150 mJ/cm² for 150 s. This step makes the photoresist not exposed in the first round of UV light soluble when introduced into the developer. The resist was then developed with a developing solution (AZ400K, Clariant Corporation) diluted in deionized (DI) water (1 : 4) for 0.8 min followed by lightly rinsing with DI water and drying with nitrogen.

The ensuing master was used as the mold to deposit the metals (Fig. 2a, metal deposition step). Using a sputter deposition system (Consolidated Vacuum Corporation), a 25 Å layer of tantalum and a 250 Å thick layer of permalloy were subsequently deposited onto the master mold. The tantalum layer helped with bonding of the permalloy to the glass wafer. The glass/silicon sandwich was then cut along cutting lines defined in the photomask to produce coverglass-like pieces that fit into a custom-made coverglass holder. The cut, coverglass-sized silicon pieces with deposited islands were released from the silicon wafer upon heating the wafer to 150°C. Excess photoresist and permalloy were removed by immersing the samples in acetone until the film residue completely lifted off from the glass substrate (≤ 15 min). As a final step, the glass wafers were rinsed in fresh acetone, isopropyl alcohol, and DI water. Figure 2b shows brightfield images of different fabricated islands used in this study.

Microscopy and imaging. We mounted the Helmholtz coils on an inverted optical microscope (Zeiss Axiovert 200) equipped with a halogen lamp and an oil immersion objective (Zeiss 63 \times , N.A. = 1.4). To initially find the island we used a 5 \times objective and then a 63 \times oil immersion objective. To track single magnetic beads, we diluted the magnetic particles from the manufacturing suspension (4.5 μm in diameter; Spherotech Inc.) with DI water to get 1% v/v. We captured the images using a CCD camera (Insight QE, SPOT Imaging Solutions) and analyzed the images using ImageJ and MATLAB Image processing tools.

Magnetotactic bacteria cultivation. Clones of *Magnetospirillum magneticum* strain AMB-1 (*Magnetospirillum* sp. ATCC[®] 700264) were obtained by aseptically streaking an inoculum across an agar plate containing magnetic spirillum growth media (MSGM) with the same nutrient components as the liquid media. Individual dark colonies were selected and microaerobically grown on liquid media until the beginning of the stationary phase. The liquid media contained 10.0 mL of Wolfe's Vitamin solution, 5.0 mL of Wolfe's Mineral solution, 2.0 mL of 0.01 ferric quinate, 0.45 mL of 0.1% resazurin, and various salts. These salts included 0.68 g of KH₂PO₄, 0.12 g of NaNO₃, 0.035 g of ascorbic acid, 0.37 g of tartaric acid, 0.37 g of succinic acid, and 0.05 g of sodium acetate. To prepare the 0.01 M ferric quinate, we used 0.27 g of FeCl₃, 0.19 g of quinic acid, and 100.0 mL of deionized water (DI) water. Resazurin was used as an oxidation-reduction indicator to visually monitor the level of oxygen present in the liquid media. The fading of the initial pink color of the liquid media indicated that the bacteria were in exponential growth phase. To confirm magnetic particle uptake within growing bacteria, we visually inspected the cells following placement of the screwcap culture tubes on a magnetic stirrer and observing the scattering of light, as the ambient light is reflected off these particles. We also inspected the AMB-1 with a transmission electron microscope (TEM).

Finite Element Methods Magnetics (FEMM). We ran the simulation using freeware - Finite Element Methods Magnetics (FEMM). We set up an asymmetrical 2D problem by simulating half of the Helmholtz coils as shown in 3A. We wrote an in-house Lua script (a programming language that can be interpreted by the FEMM program) to run simulations with different geometries (square, diamond and notch). We fixed the radius of the coils, the number of turns in the wire and the position of the islands and varied the current in the wire (see details of the script in the supplementary material).

- Desai, J. P., Pillarisetti, A. & Brooks, A. D. Engineering Approaches to Biomanipulation. *Annu. Rev. Biomed. Eng.* **9**, 35–53 (2007).
- Hosu, B. G., Jakab, K., Banki, P., Toth, F. I. & Forgacs, G. Magnetic tweezers for intracellular applications. *Rev. Sci. Instrum.* **74**, 4158–4163 (2003).
- Bazylnski, D. A. & Frankel, R. B. Magnetosome formation in prokaryotes. *Nat. Rev. Microbiol.* **2**, 217–230 (2004).
- Neuman, K. C. & Nagy, A. Single-molecule force spectroscopy: optical tweezers, magnetic tweezers and atomic force microscopy. *Nat. Methods* **5**, 491–505 (2008).
- Ruder, W. C. *et al.* Three-dimensional microfiber devices that mimic physiological environments to probe cell mechanics and signaling. *Lab Chip* **12**, 1775–1779 (2012).
- Smith, S. B., Finzi, L. & Bustamante, C. Direct mechanical measurements of the elasticity of single DNA molecules by using magnetic beads. *Science* **258**, 1122–1126 (1992).
- Haber, C. & Wirtz, D. Magnetic tweezers for DNA micromanipulation. *Rev. Sci. Instrum.* **71**, 4561–4570 (2000).
- Kim, K. & Saleh, O. A. A high-resolution magnetic tweezer for single-molecule measurements. *Nucleic Acids Res.* **37**, e136 (2009).
- Prass, M., Jacobson, K., Mogilner, A. & Radmacher, M. Direct measurement of the lamellipodial protrusive force in a migrating cell. *J. Cell. Biol.* **174**, 767–772 (2006).
- Winkleman, A. *et al.* A magnetic trap for living cells suspended in a paramagnetic buffer. *Appl. Phys. Lett.* **85**, 2411–2413 (2004).
- Kollmannsberger, P. & Fabry, B. High-force magnetic tweezers with force feedback for biological applications. *Rev. Sci. Instrum.* **78**, 114301–114306 (2007).
- Alenghat, F. J., Fabry, B., Tsai, K. Y., Goldmann, W. H. & Ingber, D. E. Analysis of Cell Mechanics in Single Vinculin-Deficient Cells Using a Magnetic Tweezer. *Biochem. Biophys. Res. Commun.* **277**, 93–99 (2000).
- Ruder, W. C. & LeDuc, P. R. Cells gain traction in 3D. *Proc. Natl. Acad. Sci. USA* **109**, 11060–11061 (2012).
- Martel, S., Mohammadi, M., FelfouL, O., Lu, Z. & Poupponneau, P. Flagellated Magnetotactic Bacteria as Control MRI-trackable Propulsion and Steering Systems for Medical Nanorobots Operating in the Human Microvasculature. *Int. J. Robot. Res.* **28**, 571–582 (2009).
- Matthews, B. D., LaVan, D. A., Overby, D. R., Karavitis, J. & Ingber, D. E. Electromagnetic needles with submicron pole tip radii for nanomanipulation of biomolecules and living cells. *Appl. Phys. Lett.* **85**, 2968–2970 (2004).
- Trepatt, X. *et al.* Oscillatory magnetic tweezers based on ferromagnetic beads and simple coaxial coils. *Rev. Sci. Instrum.* **74**, 4012–4020 (2003).
- Ruder, W. C. *et al.* Calcium signaling is gated by a mechanical threshold in three-dimensional environments. *Sci. Rep.* **2**, 1–6 (2012).
- Conroy, R. in *Handbook of Molecular Force Spectroscopy* (ed. Aleksandr Noy) Ch. 2, 23–96 (Springer US, 2008).
- Blakemore, R. Magnetotactic bacteria. *Science* **190**, 377–379 (1975).
- Amstad, E. *et al.* Triggered Release from Liposomes through Magnetic Actuation of Iron Oxide Nanoparticle Containing Membranes. *Nano Lett.* **11**, 1664–1670 (2011).
- Coey, J. M. D., Berkowitz, A. E., Balcells, L., Putris, F. F. & Barry, A. Magnetoresistance of Chromium Dioxide Powder Compacts. *Phys. Rev. Lett.* **80**, 3815–3818 (1998).
- Tsang, C., Heiman, N. & Lee, K. Exchange induced unidirectional anisotropy at FeMn-Ni₁₀Fe₂₀ interfaces. *Appl. Phys. Lett.* **52**, 2471–2473 (1981).
- Jiles, D. C. Review of magnetic methods for nondestructive evaluation (Part 2). *NDT Int.* **23**, 83–92 (1990).



24. Berg, H. C. Torque Generation by the Flagellar Rotary Motor. *Biophysical Journal* **68**, 163–167 (1995).
25. Pamme, N. Magnetism and microfluidics. *Lab Chip* **6**, 24–38 (2006).
26. Shevkoplyas, S. S., Siegel, A. C., Westervelt, R. M., Prentiss, M. G. & Whitesides, G. M. The force acting on a superparamagnetic bead due to an applied magnetic field. *Lab on a Chip* **7**, 1294–1302 (2007).
27. Long, M. L. & Newman, J. Image Reversal Techniques With Standard Positive Photoresist. *Proc. SPIE* **0469**, 189–193 (1984).

Author contributions

L.M.G., W.C.M. and P.R.L. designed the experiments. L.M.G. built the Helmholtz coils and the fabricated the magnetic islands. L.M.G. performed the experiments and under the guidance of W.C.M. wrote the code to run FEMM simulation. L.M.G. analyzed the data. L.M.G., P.R.L., W.C.M. and W.C.R. wrote and reviewed the manuscript.

Additional information

Supplementary information accompanies this paper at <http://www.nature.com/scientificreports>

Competing financial interests: The authors declare no competing financial interests.

How to cite this article: González, L.M., Ruder, W.C., Leduc, P.R. & Messner, W.C. Controlling Magnetotactic Bacteria through an Integrated Nanofabricated Metallic Island and Optical Microscope Approach. *Sci. Rep.* **4**, 4104; DOI:10.1038/srep04104 (2014).



This work is licensed under a Creative Commons Attribution-NonCommercial-ShareAlike 3.0 Unported license. To view a copy of this license, visit <http://creativecommons.org/licenses/by-nc-sa/3.0>